

## Allosteric antibody inhibition of human hepsin protease

Tobias KOSCHUBS\*, Stefan DENGL†, Harald DÜRR†, Klaus KALUZA†, Guy GEORGES†, Christiane HARTL†, Stefan JENNEWEIN†, Martin LANZENDÖRFER†<sup>1</sup>, Johannes AUER†, Alvin STERN‡, Kuo-Sen HUANG‡, Kathryn PACKMAN‡, Ueli GUBLER‡, Dirk KOSTREWA\*, Stefan RIES†, Silke HANSEN†, Ulrich KOHNERT†, Patrick CRAMER\* and Olaf MUNDIGL†<sup>2</sup>

\*Gene Center Munich, Department of Biochemistry, Ludwig-Maximilians-Universität (LMU) München, Feodor-Lynen-Str. 25, 81377 Munich, Germany, †Roche Diagnostics GmbH, Roche Biologics Research, Nonnenwald 2, 82377 Penzberg, Germany, and ‡Roche, 340 Kingsland Street, Nutley, NJ 07110, U.S.A.

Hepsin is a type II transmembrane serine protease that is expressed in several human tissues. Overexpression of hepsin has been found to correlate with tumour progression and metastasis, which is so far best studied for prostate cancer, where more than 90% of such tumours show this characteristic. To enable improved future patient treatment, we have developed a monoclonal humanized antibody that selectively inhibits human hepsin and does not inhibit other related proteases. We found that our antibody, hH35, potently inhibits hepsin enzymatic activity at nanomolar concentrations. Kinetic characterization revealed non-linear, slow, tight-binding inhibition. This correlates with the crystal structure we obtained for the human hepsin–hH35 antibody Fab fragment

complex, which showed that the antibody binds hepsin around  $\alpha$ 3-helix, located far from the active centre. The unique allosteric mode of inhibition of hH35 is distinct from the recently described HGFA (hepatocyte growth factor activator) allosteric antibody inhibition. We further explain how a small change in the antibody design induces dramatic structural rearrangements in the hepsin antigen upon binding, leading to complete enzyme inactivation.

**Key words:** Fab fragment, human hepsin antibody, induced conformational change, prostate cancer, transmembrane serine protease, X-ray structure.

### INTRODUCTION

Hepsin belongs to the type II transmembrane serine protease family, and is expressed in several human tissues, such as liver, kidney, prostate and thyroid [1]. Like other type II transmembrane serine proteases, it exhibits a short N-terminal cytoplasmic domain, a membrane-spanning region and a large C-terminal extracellular part, which comprises an SRCR (scavenger receptor cysteine-rich) domain and the serine protease domain [2–4]. Similarly to matriptase, hepsin is synthesized as a zymogen and undergoes autocatalytic activation through cleavage at Arg<sup>162</sup> [5]. The SRCR domain is tethered to the protease domain by non-covalent interactions and by an interdomain disulfide bond, as shown by structural analysis using X-ray crystallography [4,6,7].

A number of physiological roles have been described for hepsin, which probably correlate with its substrate selectivity. *In vitro*, the highest amidolytic activities were found to be associated with the precursors of hepsin itself, HGF (hepatocyte growth factor), the coagulation Factors VII, IX, X and XII [6], urokinase [8] and Ln-332 (laminin-332) [9].

Hepsin gained scientific and therapeutic interest predominantly through its role in cancer progression and metastasis. Several studies found hepsin to be highly overexpressed in prostate [10–16] and ovarian [17,18] cancers, as well as in renal cell carcinomas [19,20]. As hepsin expression correlates well with prostate cancer progression, it was proposed as a diagnostic marker and target for prostate cancer therapy (for a review see [1]). Indeed, two pivotal studies validate hepsin as a highly

relevant target for prostate cancer therapy. First, in a mouse model for non-metastasizing prostate cancer, overexpression of hepsin led to primary tumour progression and metastases [21]. Secondly, using a HGFA (HGF activator)-I-derived Kunitz domain-1 domain as a model inhibitor, Li et al. [22] elegantly demonstrated that hepsin directly promotes invasive tumour growth and metastases. Although the molecular mechanisms are not yet fully understood, an association with basement membrane disruption and cell motility [21] seems to emerge. It was found that hepsin activates pro-urokinase, which then degrades basement membranes and extracellular matrix components either directly or by promoting the plasminogen/plasmin pathway, thus leading to metalloprotease activation [8]. In addition, hepsin transgenic mice displayed reduced Ln-332 expression in prostate tumours, which was in turn shown to be a direct substrate of hepsin [9].

Traditionally, small molecule inhibitors for serine proteases have a long-standing history, and such inhibitors have also been described for hepsin [4,6,7]. However, owing to the structural conservation of the active site among serine proteases [23,24], therapeutic use is limited. On the other hand, the potential of antibodies to inhibit enzymes was demonstrated very early on [25], and, more recently, has specifically been demonstrated using monoclonal antibodies against human hepsin [26]. In addition to specific active-site inhibition, allosteric inhibition may lead to even greater specificity [27]. However, very few studies have been performed in which this mode-of-action is studied thoroughly for antibodies. One of these rare studies describes the allosteric inhibition of DHFR (dihydrofolate reductase) [28], another one

Abbreviations used: AMC, 7-amino-4-methylcoumarin; CDR, complementarity determining region; chH35, chimaeric hepsin antibody; FRET, fluorescence resonance energy transfer; FS293, FreeStyle 293; GFP, green fluorescent protein; HAT, human airway trypsin-like protease; HEK, human embryonic kidney; HGF, hepatocyte growth factor; HGFA, HGF activator; hH35, humanized hepsin antibody; i.v., intravenous; Ln-332, laminin-332; mAb, monoclonal antibody; mH35, murine hepsin antibody; NCS, non-crystallographic symmetry; RU, response units; SPR, surface plasmon resonance; SRCR, scavenger receptor cysteine-rich.

<sup>1</sup> This paper is dedicated to the memory of the scientific integrity, passion and dedication of Martin Lanzendörfer, who died in September 2010, while at the peak of his career.

<sup>2</sup> To whom correspondence should be addressed (email olaf.mundigl@roche.com).

concerns the inhibition of the trypsin-like serine protease HGFA [29].

In the present paper we describe the generation of a highly potent antibody directed against human hepsin. Both kinetic properties and intramolecular rearrangements of the antibody–hepsin complex reveal a (novel) mode of allosteric inhibition, which explains the high affinity and specificity of antibody hH35 (humanized hepsin antibody). Using X-ray crystallography, we studied binding of the hH35 Fab fragment to human hepsin at atomic resolution, which allows us to describe mechanistic details for hepsin inhibition. The highly efficient and selective inhibition properties of our human hepsin–hH35 antibody suggest that it may represent a valuable candidate for effective prostate cancer therapy.

## EXPERIMENTAL

### Preparation of hepsin

Human hepsin (Invitrogen, catalogue number M18930) comprising amino acid residues 45–417 was cloned into a pTT5 mammalian cell expression vector (NRC number 11266). The final construct contained an in-frame N-terminal signal sequence [derived from the human IL (interleukin)-12 p40 subunit] for secretion, followed by a six-amino-acid epitope tag ('EE-tag', EFMPME) for purification. 5'- and 3'-cloning sites added ASAA and AGSA sequences to either side of the insert.

For transient expression, 6 litres of freshly seeded FS293 (FreeStyle 293) cells ( $1 \times 10^6$  cells/ml, Invitrogen) were transfected at 37°C using a hepsin plasmid DNA–PEI (polyethylenimine) complex. Approximately 4 h later, 20% peptone was added to a final concentration of 0.5%, and the culture was incubated for 3 days at 37°C with agitation. The supernatant was harvested and protease inhibitor cocktail tablets (– EDTA) were added.

Then 3 litres of FS293 cell supernatant containing expressed recombinant EE-tagged human hepsin were sterile-filtered and loaded on to a 50 ml anti-EE antibody–Protein G Sepharose column (prepared as described in [30]) equilibrated in TBS/0.1 mM EDTA at a flow rate of 1.75 ml/min. The column was washed with TBS/0.1 mM EDTA and eluted with TBS/0.1 mM EDTA containing 100 µg/ml EE peptide. The eluant containing the hepsin zymogen was subjected to sequential concentration (100-fold) and dilution with TBS/0.1 mM EDTA, which led to proteolytic autoactivation of the hepsin zymogen to the active enzyme.

Cynomolgus and mouse hepsin were cloned, expressed and purified in a similar manner.

### Generation of antibodies against hepsin

Balb/c mice were immunized with the recombinant enzymatically active extracellular domain of the hepsin protein every 4 weeks three times followed by an i.v. (intravenous) boost on day 4 before fusion. Serum test bleeds were taken and the half-maximal serum titre was determined using hepsin protein-coated ELISA microtitre plates. Mice with a half-maximal titre of 1:12 800 were selected for the i.v. boost. At 3 days following the i.v. boost, splenocytes were harvested and fused with Ag8 myeloma cells. All animal experiments were carried out according to national and European guidelines and were approved by the local authorities. Screening for hepsin-specific antibodies was started by identifying antibodies binding to hepsin coated on to microtitre plates. Positive clones binding to immobilized hepsin were then

cultivated in serum-free medium (Hyclone ADCF-mAb, Thermo Scientific, catalogue number SH30349.02) for assessing the inhibitory potential, thus avoiding unspecific inhibition by serum-derived components.

### Expression of hepsin antibodies in mammalian cells

chH35 (chimaeric hepsin antibody) was transiently expressed in HEK (human embryonic kidney)-293 cells by transfection of the light- and heavy-chain plasmids via lipofection. Supernatant was collected 7 days after transfection and purified using Protein A.

hH35 was stably expressed in CHO (Chinese-hamster ovary) cells. Humanized light- and heavy-chain constructs were cloned into a mammalian expression vector containing glutamine synthetase as a selection marker. Transfected cells were selected with MSX (methionine sulfoximine) for stable expression of the antibody construct. Cells were screened for antibody expression in the supernatant and cloned as single cells by limited dilution. The final clone was expressed by a fed-batch shake flask culture, and the purified product was analysed to confirm mass identity. Large amounts of antibody were produced by a 20 litre fed-batch fermentation.

### Humanization and determination of hepsin antibody affinity

The murine hepsin antibody (termed mH35) was humanized [31] using the CDR (complementarity determining region) grafting method, i.e. by keeping the six loops that recognize the antigen intact and exchanging the murine framework for a human one [32]. The CDRs were identified according to the Kabat nomenclature (<http://www.kabatdatabase.com/index.html>), whereas several frameworks for both heavy and light chains were chosen from the human germline IMGT database [34]. To decide whether back mutations (maintaining murine antibody conformation) in the framework were required or whether forward mutations (to adapt to the human germline) could be applied in the CDRs, we have created a homology three-dimensional model of the mH35 variable regions. International and US patent applications have been submitted [35].

### SPR (surface plasmon resonance) analysis

For SPR analyses, approximately 1600 RU (response units) of Protein A and 700 RU of Protein G (10 µg/ml each) in 10 mM sodium acetate (pH 4.5) were immobilized on a CM5 sensor chip using the standard EDC [1-ethyl-3-(3-dimethylaminopropyl) carbodiimide]/NHS (*N*-hydroxysuccinimide) amine coupling procedure (GE Healthcare T100). Approximately 360 RU were captured from each of the following antibodies: mH35 (on Protein G), chH35 (on Protein A) and hH35 (on Protein A).

For affinity measurements, hepsin was injected at seven different concentrations ranging from 0 to 200 nM. Measurements were performed at 37°C and at a flow rate of 5 µl/min for 10 min. Dissociation was measured for 15 min. Each hepsin injection was followed by a pulse (30 s, 30 µl/min) of 0.85% H<sub>3</sub>PO<sub>4</sub> for regeneration. The 10 nM curves were measured in quadruplicate (hH35 and chH35) or triplicate (mH35). Data were evaluated using Biacore T100 evaluation software 2.0.3 and a 1:1 Langmuir model for fittings.

### Native epitope binding of hH35

HEK-293 cells were transfected using a construct encoding full-length hepsin with an N-terminal GFP (green fluorescent protein) to generate stable HEK-HPN–GFP cell lines (in this cell line

hepsin is represented by HPN). Stable cells were selected with 3  $\mu\text{g/ml}$  Geneticin (G418, Roche Applied Science, catalogue number 04727894001).

Clones were analysed by flow cytometry for hepsin expression using the intrinsic GFP fluorescence. Cell-surface binding of hH35 was determined by incubating the cells with 0.50–50.0  $\mu\text{g/ml}$  hH35 or an IgG isotype control for 45 min on ice. The cells were washed twice with PBS before incubation with Alexa Fluor<sup>®</sup> 647-conjugated goat anti-human IgG (Invitrogen), diluted 1:300 in PBS containing 1% (v/v) FBS (fetal bovine serum). After 30 min on ice, the cells were washed with PBS, and cell pellets were resuspended and antibody binding was measured on a FACS Canto (BD Biosciences).

For immunocytochemistry analysis, HEK-HPN-GFP cells were plated on to glass coverslips and grown overnight. Cells were then incubated with 5  $\mu\text{g/ml}$  hH35 for 30 min on ice, washed with PBS, fixed with 4% paraformaldehyde and counterstained with Cy3 (indocarbocyanine)-conjugated goat anti-human IgG (Jackson ImmunoResearch Laboratories). Confocal microscopy images were taken on a Leica TCS SP2/MP confocal laser-scanning microscope [at 100 $\times$ /1.46 NA (numerical aperture)]. Selective spectral detector emission band passes for each dye were used in sequential scanning mode.

### Enzymatic assays

Purified hepsin was diluted to 1 nM in assay buffer [50 mM Tris/HCl (pH 7.4), 100 mM NaCl, 0.1 mg/ml BSA and 0.02% Tween 20]. The acetyl-KQLR-AMC peptide (AMC is 7-amino-4-methylcoumarin) was synthesized with >95% purity as determined by HPLC and MS analysis [6].

For measuring amidolytic activities, hepsin and other proteases were transferred to a 384-well flat-bottomed plate (Optiplate, PerkinElmer). The acetyl-KQLR-AMC peptide (5  $\mu\text{M}$ ) was added and the enzyme reaction started. Assays contained less than 5% DMSO in a final test volume of 30  $\mu\text{l}$ . The fluorescence increase was monitored with excitation at 530 nm and emission at 572 nm on an Envision Reader at 26°C. For determination of the apparent  $K_m$  value and inhibition model, hydrolysis rates of at least six different concentrations of peptide were measured in triplicate. Rates of hydrolysis and apparent  $K_m$  values were calculated using XLFit<sup>®</sup> software (IDBS).

Progress curves of the steady-state reactions were analysed by adding 0.5 nM hepsin to a mixture of 10  $\mu\text{M}$  acetyl-KQLR-AMC peptide and 18–500 nM hH35. Fluorescence was measured on a Cary Eclipse Fluorescence Spectrophotometer for 2 min at 26°C. Monitoring of the enzyme reaction started after a delay of approximately 2 s. Rates for initial and steady-state reactions were calculated using linear regression analysis (XLFit<sup>®</sup> software, IDBS).

The release of AMC by other serine proteases was tested under the same buffer conditions as described for hepsin. The apparent  $K_m$  values for recombinant HAT (human airway trypsin-like protease), human matriptase and bovine enteropeptidase with the acetyl-KQLR-AMC peptide were calculated as described for hepsin. Recombinant HAT, human matriptase/ST14 catalytic domain and bovine enteropeptidase were obtained from R&D Systems. Trypsin (from porcine pancreas) was purchased from Merck (E.C. 3.4.21.4, Merck catalogue number 1.24590.0500).

For evaluation of the inhibition mechanism, various concentrations of hH35 (20–0.31 nM in 2-fold dilutions in triplicate) were incubated with 1 nM hepsin for 15 min. The linear rates of fluorescence increase were measured after simultaneously adding 20, 10, 5 and 2.5  $\mu\text{M}$  acetyl-KQLR-AMC peptide. Data

were fitted to the equations for tight binding inhibition using SigmaPlot<sup>®</sup> enzyme kinetic module software (Version 8.02, Systat).

### Hepsin inhibition by antibodies

For determination of inhibitory activities, hepsin (1 nM) and dilutions of antibodies were transferred to a 384-well flat-bottomed plate (Optiplate, PerkinElmer) and incubated for 30 min at 26°C. Peptide (5  $\mu\text{M}$ ) was added and the enzyme reaction started. After 40 min incubation at 26°C, the fluorescence increase was measured with excitation at 530 nm and emission at 572 nm on an Envision reader (PerkinElmer).

The percentage inhibition of hepsin activity was calculated according to the following formula:

$$\% \text{ Inhibition} = 100 \times [1 - (F_s - F_b)/(F_t - F_b)]$$

where  $F_s$  is the fluorescence signal of the sample including the antibody,  $F_b$  is the fluorescence signal in the absence of hepsin and antibody and  $F_t$  is the fluorescence signal in the presence of hepsin with no antibody. The concentration of inhibitor resulting in 50% inhibition ( $\text{IC}_{50}$ ) of the uninhibited enzyme was calculated after fitting the data to a four-parameter equation using XLFit<sup>®</sup> software (IDBS). At least three independent measurements were performed in triplicate.

### FRET (fluorescence resonance energy transfer) activity assay

The specificity of hH35 antibody across species was tested using a FRET activity assay with JA133-Z-Gln-Arg-Arg-Z-Lys-(TAMRA<sup>™</sup>)-NH<sub>2</sub> (synthesized and purified as described above) as the cleavable peptide. Purified human, rat or cynomolgus hepsin was diluted in assay buffer (see above) to a concentration of 10 nM. Peptide substrate was diluted in assay buffer to 300 nM and antibody hH35 to 0.293 nM. Then 10  $\mu\text{l}$  of diluted hepsin and antibody solutions were each added into 384-well microtitre plates and incubated at room temperature (20°C) for 30 min. Peptide substrate (10  $\mu\text{l/well}$ ) was added to each well, mixed and incubated at room temperature for 60 min. Signals were quantified by reading fluorescence (excitation at 530 nm and emission at 572 nm) on a Victor 2 reader (PerkinElmer). The percent inhibition of hepsin activity was calculated as described above.

### Preparation of hH35, hH35 Fab fragment and the hepsin-hH35 complex

Harvested cell culture supernatant was sterile-filtered through a 0.2  $\mu\text{m}$ -pore-size membrane (Millipore) prior to purification. The hH35 mAb (monoclonal antibody) was captured on a MabSelect SuRe resin (GE Healthcare), washed with 1 $\times$  PBS and eluted with 20 mM sodium citrate at pH 3.0. The hH35 mAb was further purified by size-exclusion chromatography using a Superdex 200 26/60 GL (Amersham Bioscience) column equilibrated with 20 mM histidine and 140 mM NaCl (pH 6.0).

hH35 mAb was cleaved with papain at 37°C. The cleavage was stopped by iodacetamide addition and the Fab fragment was purified by separation of the Fc fragment on a 1 ml MabSelect SuRe column (GE Healthcare). The human hepsin-hH35-Fab complex (hHepsin-hH35) was formed by mixing a 1:1.3 molar ratio and 30 min incubation at 20°C. The complex was concentrated slowly in an Amicon centrifugal filter unit (Millipore) and the buffer exchanged to 1 $\times$  TBS [50 mM Tris/HCl

(pH 7.4) and 150 mM NaCl]. Complex assembly was analysed by size-exclusion chromatography (Superose 12 column, GE Healthcare) and by SDS/PAGE.

### X-ray structure determination

Crystals of the hHepsin–hH35 complex, concentrated to 8 mg/ml, were grown at 20 °C in hanging drops over reservoirs containing 18 % PEG [poly(ethylene glycol)] 3350, 0.15 M MgSO<sub>4</sub> and 0.01 M barium chloride. Crystals were harvested by gradually adding glycerol to a final concentration of 14 % (v/v) and flash-cooling in liquid nitrogen. Diffraction data was collected in 0.25° increments and at 100 K on a PILATUS 6M detector at the Swiss Light Source SLS, Villigen, Switzerland. Data of a macroscopically twinned plate-crystal was processed using XDS and XSCALE [36]. The two major lattices of the crystals were indexed and integrated separately, and then scaled together. The hepsin substructure was determined by molecular replacement using PHASER [37] with the structure PDB 1Z8G [6] as an initial search model. HHpred [38] identified the PDB 1PKQ structure as a suitable search model for the Fab fragment, which was then used in PHASER split into individual constant and variable domains to solve the complete complex structure. The resulting electron-density map allowed for model correction and building in COOT [39]. The structure was refined with autoBUSTER [40] using NCS (non-crystallographic symmetry) restraints and TLS parameterization and has been deposited in the Protein Data Bank (PDB code 3T2N). Molecular graphics Figures were prepared using CHIMERA [41].

## RESULTS

### Generation of mouse anti-hepsin antibodies

Following mouse immunization using the enzymatically active form of human hepsin, hybridoma technology was applied in order to generate mouse anti-hepsin mAbs. By using ELISA to screen murine hybridoma supernatants on immobilized human hepsin antigen, we discovered a number of clones that exhibited strong inhibition. Clone number 35 was selected since it showed the strongest inhibition.

### Humanization of mouse anti-hepsin antibody led to increased affinity

The amino acid sequences of light- and heavy-chain complementary regions were grafted from the mouse mH35 antibody on to light and heavy human antibody frameworks, resulting in hH35 mAb (Figure 1A). Assuming three frameworks with a couple of back and forward mutations for each chain, a matrix comprising approximately 15 V<sub>H</sub> and 20 V<sub>L</sub> variants was built by combining the V<sub>H</sub>- and V<sub>L</sub>-harbouring plasmids. This approach led to the screening of more than 300 humanized candidates.

With regard to the heavy chain, one candidate was obtained by applying CDR grafting without back or forward mutation. To avoid potential glycosylation, Asn<sup>56</sup> was mutated to serine. The hH35 V<sub>H</sub> is based on the IMGT germline hVH7-4-1 [34] combined with the j element IGHJ4-03-1, where the free cysteine residue in position 82A in the V region has been mutated to a serine in order to avoid glutathione conjugation.

Since the lambda V<sub>L</sub> type is extremely close to the mouse germline mVL-1 with 99 % identity, we could not envisage back mutations based on specific matured amino acids. However, as

none of the human germline is really related to this particular mouse germline (highest identity percentage ~62 %), we used a homology three-dimensional model of the mH35 variable region to best preserve the CDR integrity. The back mutations F36V, A46G and Y49G restored the original smaller side chains surrounding CDR-H3 while maintaining antigen recognition. The back mutation P44F led to a strongly improved expression rate. The humanized variant described here is based on the human IMGT germline hVK7\_43 combined with the j element IGLJ6-01.

Our subsequent analysis showed complete inhibition of enzyme activity with mH35, chH35 and hH35 mAbs under the conditions tested (Figure 2A). Unexpectedly, we found inhibition increase by a factor of 14.7 compared with the murine antibody and by a factor of 6.7 compared with the chimaeric antibody. Sequence analysis (results not shown) revealed that this large improvement relied critically on the maintenance of the antibody light-chain residue Phe<sup>44</sup> during humanization.

We further used SPR with immobilized mH35, chH35 and hH35 antibodies and human hepsin injected at various concentrations to analyse binding association and dissociation (Figure 2B and Supplementary Figure S1 at <http://www.BiochemJ.org/bj/442/bj4420483add.htm>). We found that the chimaeric chH35 antibody exhibited medium affinity, similar to the mouse mH35 antibody, but the humanized antibody hH35 showed a significantly lower K<sub>d</sub> value. Inherent to all variants was a very low on-rate combined with a very low off-rate (Figure 2C and Supplementary Figure S1). Thus, once the antibody was bound to hepsin, it hardly dissociated within usual assay duration times. For the dissociating proportion, however, slow tight-binding kinetics were observed.

### Binding of hH35 mAb to cell-surface hepsin

Endogenous levels of hepsin in tumour cell lines are too low to be detected by flow cytometry or immunocytochemistry analysis. To study binding of hH35 on the cell surface, we established a HEK-293 cell line that stably overexpressed full-length hepsin with an N-terminal GFP fusion tag (Supplementary Figure S2 at <http://www.BiochemJ.org/bj/442/bj4420483add.htm>).

When these cells were incubated with increasing amounts of hH35, specific surface staining could be detected both by flow cytometry (Figure 3A) and confocal microscopy analysis (Figure 3B). Untransfected cells did not display any detectable binding (results not shown).

### Inhibition by hH35 mAb is specific for human hepsin

In order to test for undesired off-target effects, we tested the selectivity of our murine, chimaeric and humanized hepsin antibodies on other proteases in a peptide substrate activity assay (Figure 4A).

The K<sub>m</sub> values for cleavage of the acetyl-KQLR-AMC peptide were evaluated by using standard Michaelis–Menten kinetics. The values were within the range of ideal peptide substrates for respective enzymes (Supplementary Table S1 at <http://www.BiochemJ.org/bj/442/bj4420483add.htm>). We detected complete neutralization of human hepsin activity by our antibodies. In contrast, none of the other proteases tested (matriptase, HAT, enteropeptidase or trypsin) was significantly inhibited. We therefore conclude that our antibodies are indeed selective for hepsin.

In order to assess species cross-reactivity, we also tested the hH35 antibody on mouse and cynomolgus hepsin using an



**Figure 1 Multiple-sequence alignments of hH35 mAb variable regions and hepsin**

(A) Alignment of  $F_v$  sequences for hH35 antibody, IMGT germlines and mH35 antibody. Invariant and conserved residues are highlighted in green and yellow respectively. Residues are numbered according to the Kabat (<http://www.kabatdatabase.com/index.html>) numbering system and secondary structure elements for hH35 variable sequences are indicated above the sequence [spirals,  $\alpha$ - and  $3_{10}(\eta)$ -helices; arrows,  $\beta$ -strands; T, turns]. Residues important for humanization and CDR sequences are marked. (B) Alignment of structural conservation of hepsin, HGFA and trypsin. Additionally to the continuous hepsin numbering, loop numbers according to the chymotrypsin numbering systems are stated in parenthesis (grey) [42]. Secondary structure elements are indicated above the sequences for human hepsin in the PDB code 1Z8G structure and hHepsin-hH35 complex [spirals,  $\alpha$ - and  $3_{10}(\eta)$ -helices; arrows,  $\beta$ -strands; T, turns; lines, ordered but without secondary structure; broken lines, disordered regions]. Residues 160–166, 297–306, 343–350 and 377–382 were disordered in the hHepsin-hH35 crystal structure. Sequence alignments were created with STRAP [58] and MUSCLE [59]. Figures were prepared with ESPript [60].

activity assay (Figure 4B). The  $IC_{50}$  values clearly indicate that hH35 also inhibited cynomolgus, but not murine, hepsin protease activity.

### Mode of inhibition of hepsin by the hH35 mAb

To describe the binding behaviour of mAb hH35 in the activity assay, the progress curves of the steady-state reactions were

analysed by adding the enzyme to a mixture of peptide substrate and antibody (Figure 4C and Supplementary Table S2 at <http://www.BiochemJ.org/bj/442/bj4420483add.htm>). While the initial reaction velocity ( $v_0$ ) was only moderately affected at low concentrations of inhibitor, the steady-state velocity ( $v_s$ ) decreased as a function of the inhibitor concentration. The curved nature of the progress curves indicate a slow-binding inhibition. Steady-state experiments did not provide a definite conclusion on the inhibition mechanism. Therefore we decided

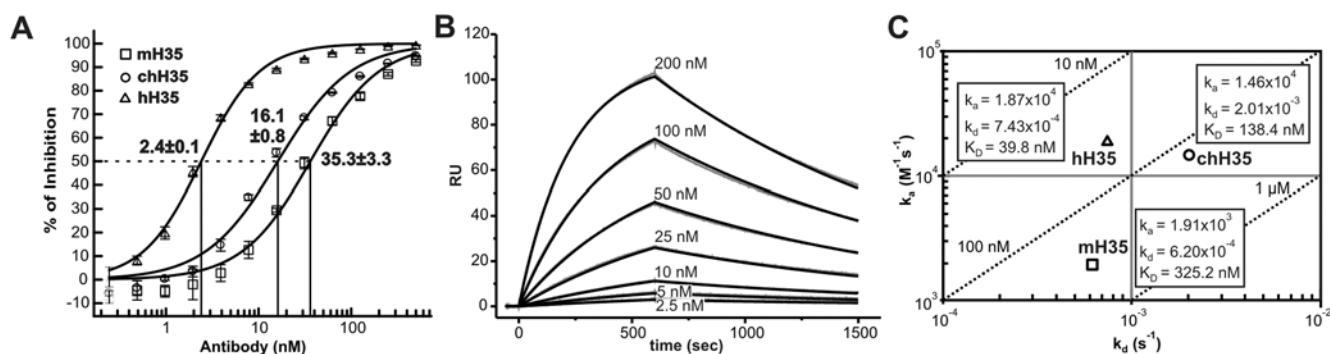


**Figure 2** Comparison of inhibition and affinity of hepsin antibodies

(A) Inhibition of hepsin activity by increasing amounts of antibody mH35 ( $\square$ ) displayed in log scale, chH35 ( $\circ$ ) and hH35 ( $\triangle$ ). After pre-incubation of the antibodies with hepsin for 30 min, the hydrolysis reaction was started by adding the acetyl-KQLR-AMC peptide. Fluorescence increase was measured after 40 min of incubation. The  $IC_{50}$  values were calculated after fitting the percentage inhibition data to a four-parameter equation. Error bars represent the S.D. for three experiments. (B) Adjusted SPR (Biacore) sensorgram analysing the binding of hepsin to the immobilized hH35 antibody. Hepsin was injected at concentrations ranging from 0 to 200 nM. Curve fittings using a 1:1 Langmuir binding model are shown by black lines. (C) Comparison of binding and dissociation constants for the mH35, chH35 and hH35 antibodies, analysed by SPR measurement and displayed in log scale.

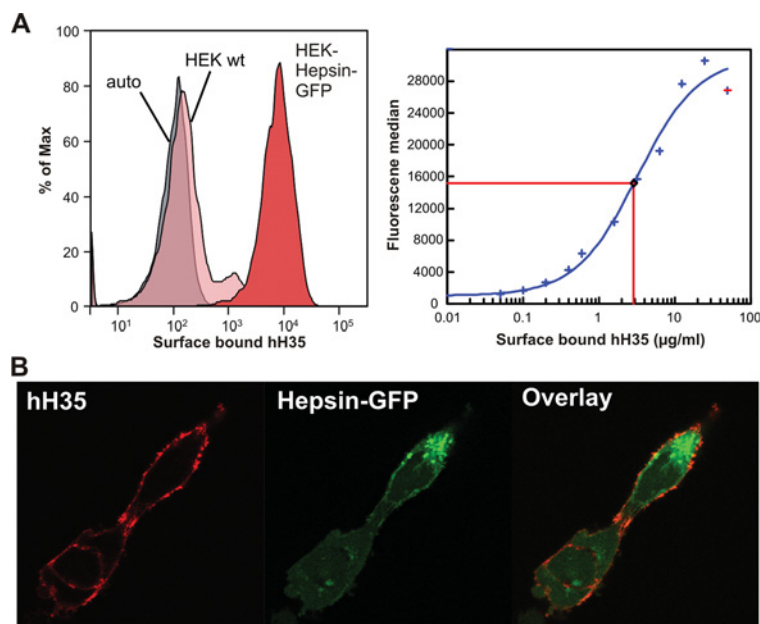


**Figure 3** Binding of hH35 to cell-surface hepsin

(A) HEK-293 cell lines that stably overexpress full-length hepsin with a C-terminal GFP fusion tag were analysed by flow cytometry. Specific and saturable surface staining could be detected by incubating with increasing amounts of hH35. (B) Hepsin surface staining by hH35 was confirmed by confocal laser-scanning microscopy analysis (red). The intrinsic fluorescence of the hepsin-GFP fusion protein is shown in green. Untransfected cells (HEK wt) did not display any detectable binding.

to first form the complex of antibody and enzyme by pre-incubation and then evaluate the inhibition model. By using non-linear least-squares regression and correction for tight-binding inhibition to determine the best-fit values, we obtained a mixed tight-binding inhibition behaviour (Supplementary Table S3 at <http://www.BiochemJ.org/bj/442/bj4420483add.htm>). As illustrated by the Eadie-Hofstee plot in Figure 4(D), the presence of increasing concentrations of hH35 significantly affected the apparent  $V_{max}$  values, whereas  $K_m$  values remained mostly unchanged ( $K_m$  change factor  $\alpha = 1.3 \pm 0.3$ ). Fitting the data to tight-binding inhibitor equations of the mixed type mechanism yielded an apparent  $K_i$  value of  $0.39 \pm 0.06$  nM.

The second most likely mechanism was non-competitive tight type inhibition, which is also common for allosteric inhibition and thus reduced affinity of the substrate for the active centre.

#### Structure of the hHepsin-hH35 complex reveals recognition of hepsin in a deep and hydrophobic pocket

The crystal structure solution for the extracellular part of human hepsin revealed a classical serine-protease domain accompanied by an SRCR domain [4].

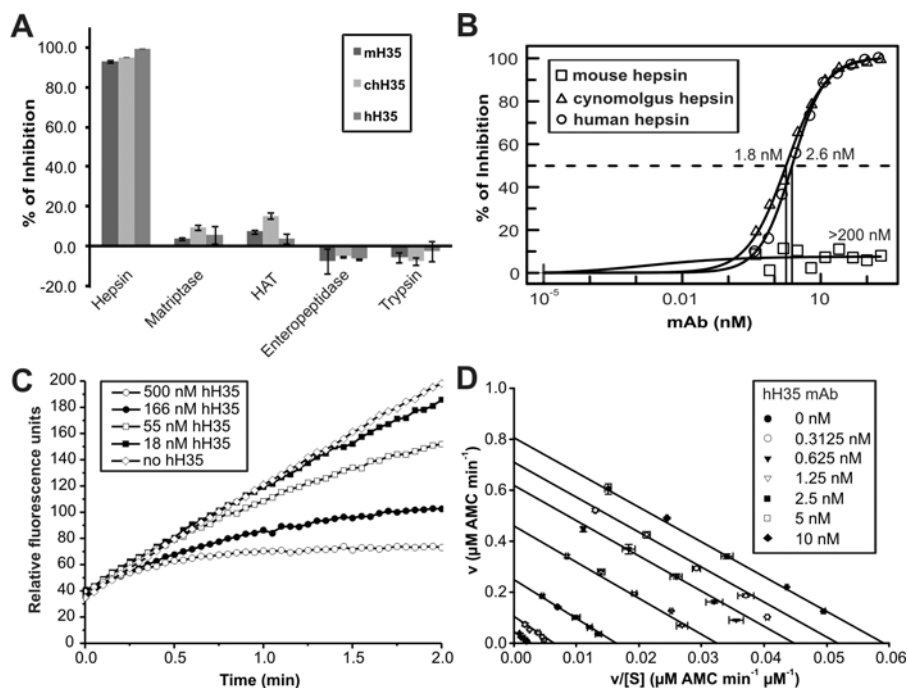


**Figure 4** mAb hH35 is protease- and species-specific and exhibits non-linear inhibition

(A) Activity of hepsin antibodies against other serine proteases. The same test conditions were used for assessing the inhibitory potential of the antibodies on other serine proteases as were used for hepsin. Hepsin (1 nM), matriptase (2 nM), HAT (2 nM), enteropeptidase (0.7 nM) and trypsin (1.8 nM) were incubated with antibody (500 nM) for 30 min and the reaction was started with 5  $\mu$ M acetyl-KQLR-AMC peptide. Data are shown for three replicate experiments. (B) Activity of antibody hH35 analysed in a FRET activity assay against human, cynomolgus and mouse hepsin. Cross reactivity was found with cynomolgus, but not with mouse hepsin.  $IC_{50}$  values are stated accordingly. (C) Progress curve of hepsin inhibition by hH35 mAb. Hepsin (0.5 nM) was added to a mixture of acetyl-KQLR-AMC peptide (10  $\mu$ M) and 0, 18, 55, 166 and 500 nM hH35 mAb. The increase in fluorescence was monitored at 3-s intervals over 2 min. Rates for initial ( $v_0$ ) and steady-state ( $v_s$ ) reactions were calculated using linear regression analysis. (D) Eadie-Hofstee plot of hepsin inhibition by hH35 mAb. Hepsin (1 nM) was pre-incubated without (●) or with hH35 mAb (20–0.31 nM in 2-fold dilution steps) for 15 min. After the addition of acetyl-KQLR-AMC peptide (40, 20, 10, 5 and 2.5  $\mu$ M) the linear rates of the increase in fluorescence were measured on a kinetic microplate reader. The graph shows the plot for the top-ranked mixed tight inhibition model ( $V_{max} = 0.81 \pm 0.01$   $\mu$ M AMC/min and  $K_m = 13.65 \pm 0.44$   $\mu$ M for control;  $\alpha = 1.3 \pm 0.3$ ). Data are plotted as means  $\pm$  S.D. for  $n = 3$ .

The 2.55 Å (1 Å = 0.1 nm) hHepsin-hH35 complex structure (Table 1, and Figures 1 and 5) has now revealed that the major epitope of hepsin for the hH35 antibody is located around the hepsin  $\alpha$ 3-helix and adjacent residues (loop-170 according to the chymotrypsin numbering system [42]). This protruding helix and following residues are located far from both the active centre and the SRCR domain.

Superimposition of human hepsin in complex with hH35 (the present study) and human hepsin bound to the peptide inhibitor substrate (PDB code 1Z8G) revealed minor and major differences (Figure 6B). First, the SRCR domain was slightly skewed. The major observed difference, however, was the active centre for which a few regions could not be built due to weak or missing electron density. As indicated in Figure 1(B) and by the dotted lines in Figure 5(B), three of these loops (Gly<sup>297</sup>-Ala<sup>306</sup>, Glu<sup>343</sup>-Gln<sup>350</sup> and Trp<sup>377</sup>-Ala<sup>382</sup>) (loops-140, -190 and -220) are located in a defined region of the protease domain. This was apparently not due to crystal packing forces, since we detected this in both NCS copies (Supplementary Figure S3A at <http://www.BiochemJ.org/bj/442/bj4420483add.htm>). These residues were not located close to any crystal contacts that may have caused this artificially (Supplementary Figure S4 at <http://www.BiochemJ.org/bj/442/bj4420483add.htm>). These loops thus most probably represent flexible regions, which is a frequent cause of blurred electron density in X-ray crystallography. Since equal regions were ordered in crystal structures without the Fab fragment [4,6,7], we concluded that the observed disorder is induced upon antibody binding.

While some hepsin loops were missing in the structure model, all antibody CDR loops could be built in the complex (Figure 5C). Most importantly, hepsin residues Phe<sup>327</sup>-Tyr<sup>328</sup> (from the 170-loop) were recognized by antibody hH35 in a deep hydrophobic pocket that was formed by both heavy- and light-chain CDRs and neighbouring residues (Figure 5B). In addition to the dominant hydrophobic interactions, some side-chain and backbone hydrogen bonds also make significant contacts at the binding interface. A detailed analysis of all contacts between hepsin and hH35 Fab can be found in Supplementary Figure S4.

#### Formation of the hepsin recognition pocket is induced by Phe<sup>44</sup> in hH35 V<sub>L</sub>

Since formation of such a deep hydrophobic recognition pocket is unusual for antibodies, we sought to explain its formation in more detail and analysed the differences between hH35 Fab and other published Fab fragment structures. mAb hH35 did not exhibit the conventional double or single hydrogen bond between V<sub>H</sub> Gln<sup>39</sup> and V<sub>L</sub> Gln<sup>38</sup> or Glu<sup>38</sup> residues. This is illustrated by superimposing the PDB 1NL0 structure, which was chosen as an example due to very similar Fab fragment elbow angles (Figure 6A). Instead, the distance between these two residues is widened by approximately 2 Å due to hH35 V<sub>L</sub> residue Phe<sup>44</sup>. The Phe<sup>44</sup> residue from the mouse antibody was maintained during humanization, although 95 % of the human germlines display a Pro<sup>44</sup> residue. This not only caused the central interface between

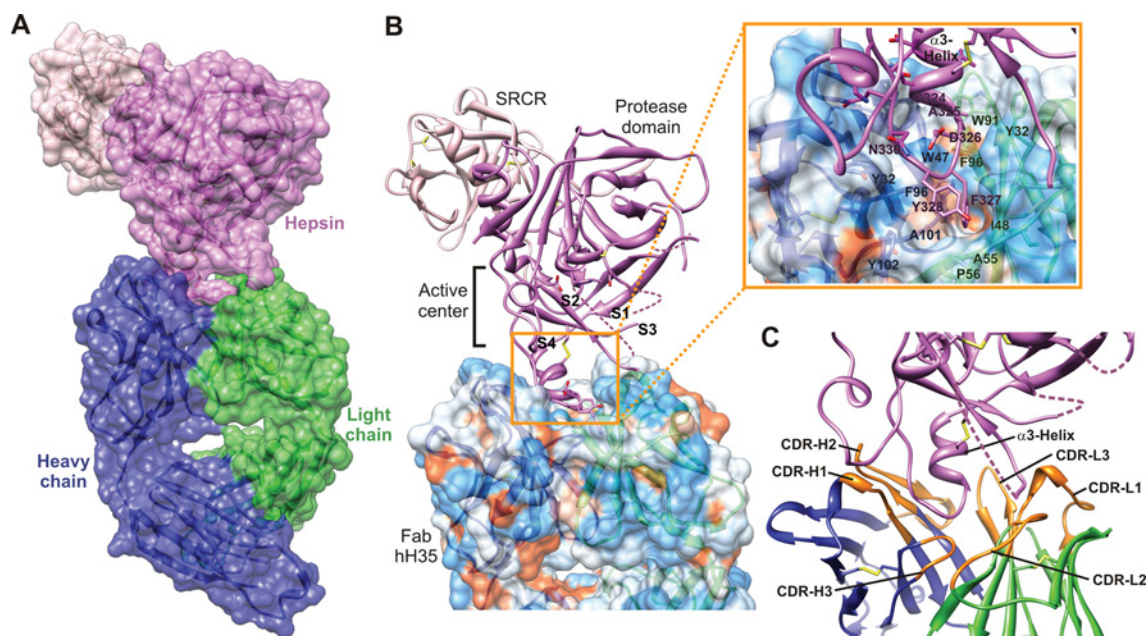


**Figure 5** Analysis of the hHepsin-hH35 Fab complex structure

(A) Surface view of human hepsin in complex with the hH35 Fab fragment. The protease domain of human hepsin is shown in violet and the SRCR domain is shown in light violet. Heavy and light chains of the hH35 Fab fragment are shown in blue and green respectively. The surface is semi-transparent to show the underlying structure. (B) Residues following the human hepsin  $\alpha$ 3-helix reach into a specific, deep and hydrophobic pocket formed by hH35. The hydrophobicity surface of hH35 Fab is semi-transparent in this Figure, with colours ranging from dodger blue for the most hydrophilic to white at 0.0, and to orange-red for the most hydrophobic. The substrate-binding pocket (marked by S1–S4) is not covered by the antibody, but the antibody forms itself a binding pocket. A close-up of this pocket illustrates the involved contact residues. (C) Ribbon model illustration of antibody CDRs (H1–H3 and L1–L3) shown in orange. Disordered parts in the crystal structure are indicated by broken lines.

**Table 1** Data collection and refinement statistics from hHepsin-hH35 crystal structure determination

Values in parentheses are for the highest-resolution shell. RSCC, real space cross-correlation; Rmsd, root mean square deviation.

Measurement	
Data collection	
Space group	$P_1$
Unit cell parameters	
a, b, c (Å)	63.0/66.6/108.3
$\alpha, \beta, \gamma$ (°)	88.7/94.3/104.5
Wavelength (Å)	0.987
Resolution range (Å)	47.33–2.55 (2.55–2.62)
Unique reflections	54655
Completeness (%)	98.7 (99.1)
Redundancy	3.4 (3.6)
$R_{\text{sym}}$ (%)	13.1 (68.9)
$I/\sigma I$	7.98 (2.17)
Model refinement	
Number of atoms	
Protein	11434
Water	315
Number of residues	1505
$R_{\text{work}}, R_{\text{free}}$ (%)	24.3, 27.5
RSCC main, side†	0.918, 0.816
Rmsd	
Bond length (Å)	0.011
Bond angle (°)	1.24
B-factor average (Å <sup>2</sup> )	48.3
Ramachandran plot (%) (favoured/allowed/outlier)	97.1/2.6/0.3
*5 % of the data were set aside for free $R$ -factor calculation.	
†Real space cross correlation coefficients as calculated by autoBUSTER [40].	

heavy and light variable regions to widen, but also has a leverage effect that induces further CDR movements (Figure 6A) and forms the highly defined recognition pocket illustrated in Figure 5(B).

### The hHepsin-hH35 atomic structure explains antibody specificity

As shown in Figure 4, the hH35 antibody was both specific for the hepsin-type protease and species-specific for hepsin as well. These findings result from the unique sequence of the hH35-specificity determining region in human hepsin (Figure 1B, black bar). Other proteases, such as HGFA, matriptase or trypsin, do not possess a Phe<sup>327</sup>Tyr<sup>328</sup> motif (in the 170-loop) that could insert into the recognition pocket to the same extent (Figure 5B). Secondly, the overall conformation and flexibility of the (170-) loop following the  $\alpha$ 3-helix must be different since the Gly<sup>324</sup>Ala<sup>325</sup> motif occurs only in human and monkey hepsin, but not in rodents or other more distant species. Instead, a serine-proline motif is often present, which typically leads to a proline-induced kink in the structure.

### Mechanism of inhibition

The most obvious allosteric change in human hepsin upon hH35 binding was the turn of the Phe<sup>327</sup>Tyr<sup>328</sup>-motif-containing loop (170-loop, following the  $\alpha$ 3-helix) towards the antibody cleft (Figure 6B). Helix  $\alpha$ 3 and sheet  $\beta$ 18 are held still in a position similar to that in the hepsin-peptide-substrate complex structure (PDB code 1Z8G), which may be explained by the disulfide bond between residues Cys<sup>322</sup> and Cys<sup>338</sup>. The hepsin loop regions 342–344 (190-loop) and 382–386 (220-loop) would clash with the hH35 V<sub>L</sub> chain in case that they adopted the same conformation

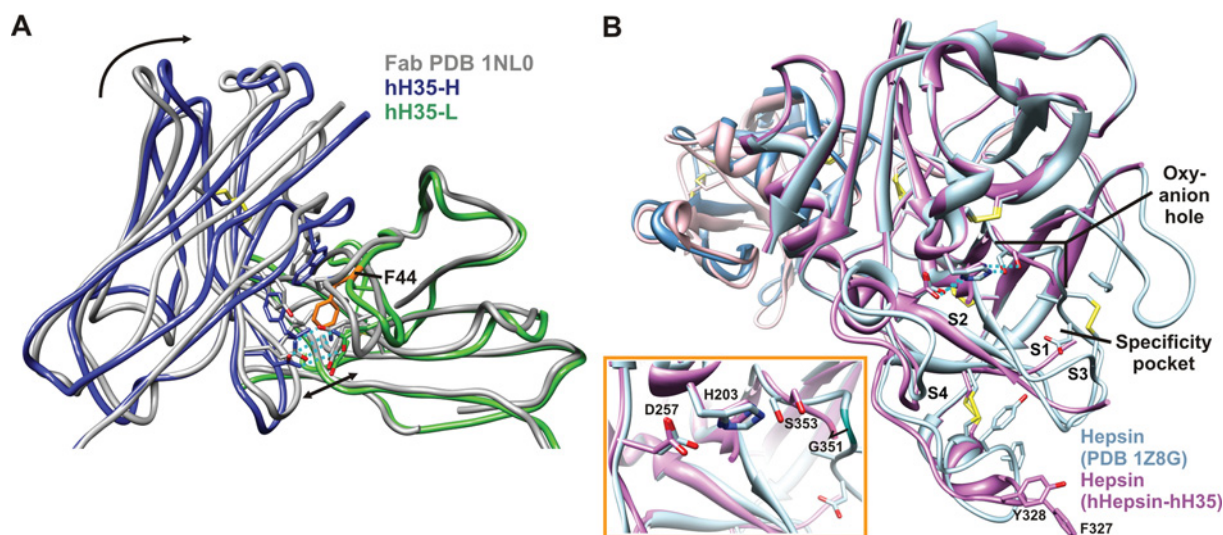


**Figure 6** Induced structural movements

(A) Structure of hH35  $V_L$  superimposed on the PDB code 1NLO structure [61]. Usually, residues  $V_H$  (left-hand side) Gln<sup>39</sup> and  $V_L$  (right-hand side) Gln<sup>40</sup> (or equivalent) form a double hydrogen bond at approximately 2.9 Å distance, as illustrated by the PDB code 1NLO structure in grey. Residue  $V_L$  Phe<sup>44</sup> (orange) widens this hydrogen bond distance to approximately 5.2 Å in the hHepsin-hH35 structure. This leads to structural rearrangements creating a recognition pocket for human hepsin at the top cleft between the  $V_L$  (green) and  $V_H$  (blue) chains. (B) Ribbon model of human hepsin in the hHepsin-hH35 complex structure superimposed with human hepsin in the PDB code 1Z8G structure. The catalytic triad Asp<sup>257</sup>-His<sup>203</sup>-Ser<sup>353</sup> and other important residues are represented as sticks. Hydrogen bonds (broken blue lines) are omitted in the close-up view of the catalytic triad for clarity. Substrate-binding pockets are marked by S1-S4.

as in the hepsin structure PDB code 1Z8G. As a consequence, the affected residues propagated partially to newly defined positions and, to a greater extent, into flexible conformations. This is reflected by the lack of electron density for loop residues 343-350 (190-loop) and 377-382 (220-loop), which are connected by a disulfide bond as well and thus adapt concurrently. Near the end of the disordered 343-350 (190-loop) loop, residue Asp<sup>352</sup> (which is the amino acid residue next to the catalytic Ser<sup>353</sup>) changed conformation. In structures PDB code 1Z8G and PDB code 1P57, residue Asp<sup>352</sup> is in contact with the backbone nitrogen of Ile<sup>163</sup> via its oxygen O<sup>δ2</sup>. In our structure, Asp<sup>352</sup> has flipped, making contact with the N<sup>ε2</sup> nitrogen from His<sup>186</sup>. Since electron density was not sufficient to build the Ile<sup>163</sup> residue, increased flexibility of this binding partner might be the cause of the conformational change. We noticed, however, that the contact distance stayed the same (at 2.7 Å), arguing for the inter-changeability between both conformations, which may have relevance for autocatalytic hepsin cleavage after Arg<sup>162</sup>.

Another result of the latter conformational change is the twist in the backbone bearing the catalytic triad residue Ser<sup>353</sup> (Figure 6B, inset). For the nucleophilic attack of the carbonyl carbon on the scissile bond, the catalytic triad serine oxygen O<sup>γ</sup> must be oriented at an angle of exactly 109° [24]. As such, we conclude that proteolytic cleavage can no longer take place (Figure 6B, inset). Residues Asp<sup>257</sup> and His<sup>203</sup> of the catalytic triad are slightly distorted as well, but to a lesser extent than Ser<sup>353</sup> (Figure 6B and Supplementary Figure S3B).

Aside from changes in the active centre, the catalytic and substrate-binding pockets were heavily disordered in our structure as well (Figure 6B and Supplementary Figures S3C and S3D). The orientation of the oxyanion hole residue Gly<sup>351</sup> is changed in a way that would hamper stabilization of the catalytic tetrahedral intermediate state. Substrate binding pockets S2 and S4 are slightly distorted in our structure, and substrate-binding pockets S1 (including the specificity pocket) and S3 are almost completely disordered (Supplementary Figures S3C and S3D). In summary, inhibition by hH35 binding results both from distorted hepsin

geometry, especially at the catalytic triad, and from disordered binding pockets, which probably dramatically reduce the affinity of substrates.

### Recognition of hepsin by antibody hH35 is different from published anti-HGFA antibodies

Owing to the generally planar or concave antigen-binding site shape, antibodies were originally thought to be ill-suited for inhibition of proteases, which exhibit a concave-shaped substrate-binding cleft [43]. Nevertheless, it has been shown for HGFA that complete competitive inhibition of a protease by an antibody is possible (Figure 7A and [43]), although not easy to achieve. In this case, the concave-shaped  $V_H$  and  $V_L$  of HGFA-Fab58 bind to the convex-shaped 99-loop of HGFA [43], which is similar to the concave-shaped  $V_H$  and  $V_L$  of hH35 that embrace a convex element (the 170-loop) of hepsin. While very long CDR loops may be an alternative to solve this dilemma, allosteric antibody inhibition has been explored for the first time for serine proteases. HGFA [29] was also used as an example here.

Similar to the HGFA-Fab40 structure (Figure 7B), the epitope region in the structure of hHepsin-hH35 (Figure 7C) is located far from the active-centre cleft, thus suggesting an allosteric mechanism of inhibition. However, this mechanism is distinct from that found for HGFA-Fab40, as very distant (and therefore different) regions are bound by the particular antibodies for hepsin and HGFA (Figures 7B and 7C). In fact, superimposing hepsin and HGFA structures demonstrates that allosteric inhibition of serine proteases by antibodies is not limited to certain trigger spots, but can instead exploit diverse enzyme surface regions.

### DISCUSSION

According to the GLOBOCAN study in 2008 (<http://www.globocan.iarc.fr>), prostate cancer is the second most common

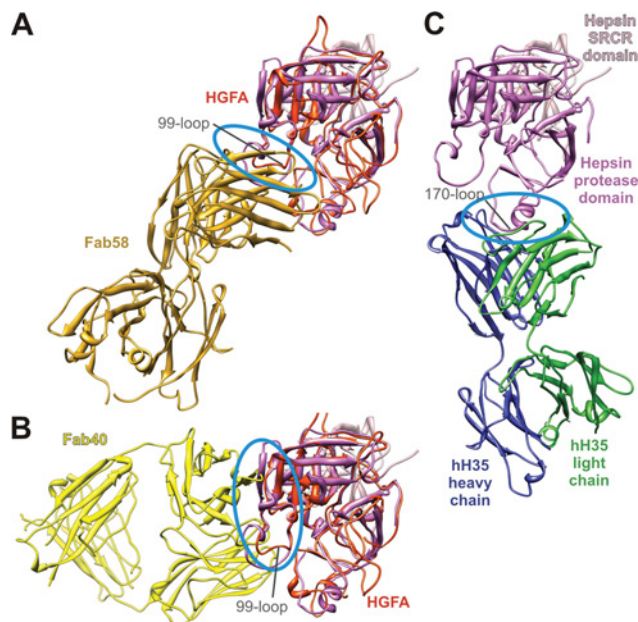


**Figure 7** Comparison of recognition regions with published HGFA–Fab complex structures

(A) Ribbon model of human hepsin (violet and light violet) superimposed on the PDB code 2R0K structure [43]. Human HGFA is shown in red and the antibody Fab58 fragment is in ochre. The HGFA–Fab58 epitope area is marked with a cyan circle. (B) Ribbon model of human hepsin (violet and light violet) superimposed on the PDB code 3K2U structure [29]. Human HGFA is shown in red and the antibody Fab40 fragment is shown in yellow. The HGFA–Fab40 epitope area is marked with a cyan circle. (C) Ribbon model representation of the hHepsin–hH35 complex. Colour coding is the same as in Figures 1 and 5. The epitope region is located approximately 15–20 Å away from the hepsin active-centre cleft. The hHepsin–hH35 epitope area is marked with a cyan circle.

cancer in men worldwide. While this number may be partially biased due to increased screening efforts, prostate cancer still remains the second most common cause of cancer death in developed countries. More extensive diagnosis and treatment has led to an increase in long-term survival rate, but a huge effort is still needed to significantly improve treatment and to cope with this type of cancer, especially in aging populations. In the present paper we describe an antibody directed against human hepsin (named hH35) that uses an allosteric mode-of-action to achieve full inhibition at nanomolar concentrations. This antibody also functionally binds to native hepsin on the cell surface and is highly hepsin specific.

Analyses of binding mode details consisted of biophysical, kinetic and structural investigations. Kinetic studies on the binding of hH35 to the enzyme revealed a slow on- and off-rate for binding of hH35 to hepsin. The initial inhibition of enzyme activity indicated a slow onset of hepsin inhibition by hH35, which is typical for slow-binding inhibition [45,48]. The nature of this inhibition suggests a multistep mechanism, most probably due to allosteric influences. In order to further elucidate the allosteric nature of this inhibition we studied the complex by X-ray crystallography, and indeed, the crystal structure of the hHepsin–hH35 complex revealed that binding of the hH35 antibody appears approximately 15–20 Å away from the active centre, thereby inducing allosteric changes through a cascade of conformational changes. This is mediated in hepsin by the turn of the Phe<sup>327</sup>Tyr<sup>328</sup>-motif-containing loop (170-loop, following the  $\alpha$ 3-helix) towards the antibody cleft.

The completeness of inhibition probably resulted from the distortion of the active centre and from the disorder of the binding

pockets. This may also explain why we could not absolutely distinguish between mixed-mode and non-competitive tight-binding inhibition. A more detailed investigation would require elaborate studies, such as a stopped-flow analysis. It is quite possible, however, that additional steric hindrance by the bound antibody can occur for the macromolecular natural substrates. Moreover, our crystal structure provides a clearer explanation for the tightness of the binding, which appeared to crucially depend on the presence of the large and hydrophobic V<sub>L</sub> Phe<sup>44</sup> residue. This residue widened the distance between V<sub>H</sub> Gln<sup>39</sup> and V<sub>L</sub> Gln<sup>38</sup>, which usually form a double hydrogen bond. The leverage movement then propagates to the top cleft between the V<sub>H</sub> and V<sub>L</sub> antibody chains, where a deep and narrow binding pocket is formed. One unexpected result of the humanization is the affinity and specificity increase for human hepsin that can best be explained by the specific allosteric movement of the hepsin Phe<sup>327</sup>Tyr<sup>328</sup> loop (170-loop). In rodents, this change is prohibited by different conformations and possibly by the flexibility of the loop, especially due to hepsin residues 324–325 (serine–proline). An increase in affinity due to conformational changes of the antigen has been observed before, as in the case of the antibody–rheumatoid factor complex [44].

A series of well-recognized studies on protease inhibition by antibodies was conducted for HGFA [29,43,45], for which pro-HGF is a natural substrate as well (as it is for hepsin). In findings similar to those of the present study, the crystal structure of the HGFA–Fab40 complex exhibited an allosteric mode of inhibition. Structural alignment clarified, however, that the recognized regions are very distinct. This also applies to the actual allosteric mechanism leading to protease inhibition. In the case of the Ab40 HGFA antibody, the 99-loop is sandwiched between the substrate and the antibody-binding side, serving as a mobile conduit between these sites. Antibody H3 residue Trp<sup>95</sup> is inserted into a large hydrophobic pocket of HGFA and locks the 99-loop in a non-competent conformation characterized by a partial collapse of the S2 pocket and loss of stabilizing P4–S4 interactions [45]. The conformation of the catalytic triad is not significantly changed in comparison with other known structures of HGFA [29]. We found a different situation for antibody hH35, where hydrophobic antigen residues insert into a hydrophobic pocket on the antibody surface. In addition to the heavy disorder of pockets S1 and S3 and the small changes in pockets S2 and S4, we recognized a distortion in the conformation of the catalytic triad residues. To our knowledge, the structure shown in the present study is the first example of such a rearrangement induced by an antibody.

However, misplacement of the catalytic triad is not uncommon for the modulation of enzymatic activity. One well-described example is the allosterically regulated bacterial trypsin-like protease DegS showing that binding of its PDZ domain to the protease domain induces disorder in several important loops and a subtle increase in the distance of the active-site histidine and serine by only ~1–2 Å, thus rendering the enzyme inactive. Upon binding of activating peptides the two residues move into the geometrically correct positions, which activates the protease [46,47]. Other examples of enzyme inhibition by altered active-site geometry apart from serine proteases have been described [48,49]. Another well-documented example is the exosites on Factor VIIA, where binding of small inhibitory peptides leads to complete enzymatic inhibition by distorting the oxyanion hole [50].

In addition to antigen-induced conformational change of the antibody upon binding [51], antibody-induced conformational change of the antigen upon binding is likewise a well-known phenomenon [53,54]. To the best of our knowledge, however,

strong disorder of the antigen induced by an antibody has not yet been observed. The present study should therefore be considered as unique in that respect. More common examples are those in which the antibody orders antigen conformation, especially in antigens that are naturally disordered. Adopting this kind of conformation results from a shift in native state probability upon ligand binding [52]. In this respect, the observed hepsin structure may represent a native state that becomes energetically most favourable. Interestingly, the existence of distinct low-energy states in equilibrium was recently described for trypsin-like proteases [53].

Allosteric regulation is very widespread in nature, and applies to areas such as enzymatic activity regulation [54], receptor signalling [55] and even regulation of gene transcription [56]. To date, however, most enzyme inhibitors are small molecules and target the active sites of enzymes. But this is especially unfavourable in the case of proteases. Active-site topologies, for instance, are often well-conserved among distinct proteases and thus difficult to address selectively by small molecules. Secondly, these inhibitors frequently mimic the transition state of enzyme catalysis with often undesirable pharmacokinetic properties [23]. Thus, especially for the protease enzyme class, there is an unmet need for alternative inhibitors, such as inhibitory antibodies. Active-site inhibition using antibodies with a very long CDR-loop reaching into the active-centre cleft may be an alternative, as shown for the type II transmembrane serine-protease matrilysin [57] and for HGFA [43], but may be restricted in use to only one or two CDR loops. In contrast, allosteric inhibition as described in the present study may use the full variability spectrum of all CDRs.

In conclusion, the findings of the present study demonstrate a potent and unique mode of inhibition by a novel anti-hepsin antibody that may enable improved treatment options to prevent cancer progression in human patients.

## AUTHOR CONTRIBUTION

The work was carried out as a collaborative effort among all authors. Olaf Mundigl, Kathryn Packman, Stefan Ries and Silke Hansen defined the project strategy and supervised antibody generation and biochemical/functional characterization. Ulrich Kohnert, Patrick Cramer and Harald Dürr initiated and supervised the generation and characterization of the crystal structure. Alvin Stern, Kuo-Sen Huang and Ueli Gubler generated and characterized the different hepsins used in the study. Olaf Mundigl generated the murine anti-hepsin antibodies and HEK-hepsin cell line, and performed the FACS and immunocytochemistry assays. Klaus Kaluza designed and performed kinetic and specificity assays. Christiane Hartl, Stefan Jennewein and Martin Lanzendörfer performed the Biacore analysis. Guy Georges and Johannes Auer modelled and designed the humanization of the anti-hepsin antibody. Stefan Dengl prepared and crystallized the hHepsin-hH35 complex. Tobias Koschubs determined the hHepsin-hH35 crystal structure. Dirk Kostrewa advised on structure solution and Guy Georges provided support for structure interpretation. Tobias Koschubs, Patrick Cramer and Olaf Mundigl wrote the paper with contributions from all co-authors.

## ACKNOWLEDGEMENTS

We thank Jan Olaf Stracke (Roche Penzberg) for making analytical evaluation possible. We also thank Judith Gerlach, Ranjan Sircar, Monika Heidrich, Heike Seul and Doris Ziegler-Landesberger for their excellent technical assistance. At the Gene Center Munich, we would like to thank the Cramer laboratory members Kerstin Kinkelin, Fuensanta Martinez and Sarah Sainsbury for their crystal measurements. We also acknowledge the crystallization facility within E. Conti's department at the Max Planck Institute of Biochemistry, Martinsried, for initial crystal screening. Part of this study was performed at the Swiss Light Source (SLS) at the Paul Scherrer Institute (Villigen, Switzerland).

## FUNDING

S.D., H.D., K.K., G.G., Ch.H., S.J., M.L., J.A., A.S., K-S.H., K.P., U.G., S.R., S.H., U.K., O.M. are or were all employees of Roche.

## REFERENCES

- Wu, Q. and Parry, G. (2007) Hepsin and prostate cancer. *Front. Biosci.* **12**, 5052–5059
- Hooper, J. D., Clements, J. A., Quigley, J. P. and Antalis, T. M. (2001) Type II transmembrane serine proteases. Insights into an emerging class of cell surface proteolytic enzymes. *J. Biol. Chem.* **276**, 857–860
- Leytus, S. P., Loeb, K. R., Hagen, F. S., Kurachi, K. and Davie, E. W. (1988) A novel trypsin-like serine protease (hepsin) with a putative transmembrane domain expressed by human liver and hepatoma cells. *Biochemistry* **27**, 1067–1074
- Somoza, J. R., Ho, J. D., Luong, C., Ghate, M., Sprengeler, P. A., Mortara, K., Shrader, W. D., Sperandio, D., Chan, H., McGrath, M. E. and Katz, B. A. (2003) The structure of the extracellular region of human hepsin reveals a serine protease domain and a novel scavenger receptor cysteine-rich (SRCR) domain. *Structure* **11**, 1123–1131
- Qiu, D., Owen, K., Gray, K., Bass, R. and Ellis, V. (2007) Roles and regulation of membrane-associated serine proteases. *Biochem. Soc. Trans.* **35**, 583–587
- Herter, S., Piper, D. E., Aaron, W., Gabriele, T., Cutler, G., Cao, P., Bhatt, A. S., Choe, Y., Craik, C. S., Walker, N. et al. (2005) Hepatocyte growth factor is a preferred *in vitro* substrate for human hepsin, a membrane-anchored serine protease implicated in prostate and ovarian cancers. *Biochem. J.* **390**, 125–136
- Katz, B. A., Luong, C., Ho, J. D., Somoza, J. R., Gjerstad, E., Tang, J., Williams, S. R., Verner, E., Mackman, R. L., Young, W. B. et al. (2004) Dissecting and designing inhibitor selectivity determinants at the S1 site using an artificial Ala190 protease (Ala190 uPA). *J. Mol. Biol.* **344**, 527–547
- Moran, P., Li, W., Fan, B., Vij, R., Eigenbrot, C. and Kirchhofer, D. (2006) Pro-urokinase-type plasminogen activator is a substrate for hepsin. *J. Biol. Chem.* **281**, 30439–30446
- Tripathi, M., Nandana, S., Yamashita, H., Ganesan, R., Kirchhofer, D. and Quaranta, V. (2008) Laminin-332 is a substrate for hepsin, a protease associated with prostate cancer progression. *J. Biol. Chem.* **283**, 30576–30584
- Dhanasekaran, S. M., Barrette, T. R., Ghosh, D., Shah, R., Varambally, S., Kurachi, K., Pienta, K. J., Rubin, M. A. and Chinnaiyan, A. M. (2001) Delineation of prognostic biomarkers in prostate cancer. *Nature* **412**, 822–826
- Ernst, T., Hergenroth, M., Kenzelmann, M., Cohen, C. D., Bonrouhi, M., Wening, A., Klaren, R., Groner, E. F., Wiesel, M., Gudemann, C. et al. (2002) Decrease and gain of gene expression are equally discriminatory markers for prostate carcinoma: a gene expression analysis on total and microdissected prostate tissue. *Am. J. Pathol.* **160**, 2169–2180
- Luo, J., Duggan, D. J., Chen, Y., Sauvageot, J., Ewing, C. M., Bittner, M. L., Trent, J. M. and Isaacs, W. B. (2001) Human prostate cancer and benign prostatic hyperplasia: molecular dissection by gene expression profiling. *Cancer Res.* **61**, 4683–4688
- Magee, J. A., Araki, T., Patil, S., Ehrig, T., True, L., Humphrey, P. A., Catalona, W. J., Watson, M. A. and Milbrandt, J. (2001) Expression profiling reveals hepsin overexpression in prostate cancer. *Cancer Res.* **61**, 5692–5696
- Stamey, T. A., Warrington, J. A., Caldwell, M. C., Chen, Z., Fan, Z., Mahadevappa, M., McNeal, J. E., Nolley, R. and Zhang, Z. (2001) Molecular genetic profiling of Gleason grade 4/5 prostate cancers compared to benign prostatic hyperplasia. *J. Urol.* **166**, 2171–2177
- Stephan, C., Yousef, G. M., Scorilas, A., Jung, K., Jung, M., Kristiansen, G., Hauptmann, S., Kishi, T., Nakamura, T., Loening, S. A. and Diamandis, E. P. (2004) Hepsin is highly over expressed in and a new candidate for a prognostic indicator in prostate cancer. *J. Urol.* **171**, 187–191
- Welsh, J. B., Sapinoso, L. M., Su, A. I., Kern, S. G., Wang-Rodriguez, J., Moskaluk, C. A., Frierson, Jr, H. F. and Hampton, G. M. (2001) Analysis of gene expression identifies candidate markers and pharmacological targets in prostate cancer. *Cancer Res.* **61**, 5974–5978
- Adib, T. R., Henderson, S., Perrett, C., Hewitt, D., Bourmpoulia, D., Ledermann, J. and Boshoff, C. (2004) Predicting biomarkers for ovarian cancer using gene-expression microarrays. *Br. J. Cancer* **90**, 686–692
- Tanimoto, H., Yan, Y., Clarke, J., Korourian, S., Shigemasa, K., Parmley, T. H., Parham, G. P. and O'Brien, T. J. (1997) Hepsin, a cell surface serine protease identified in hepatoma cells, is overexpressed in ovarian cancer. *Cancer Res.* **57**, 2884–2887
- Betsunoh, H., Mukai, S., Akiyama, Y., Fukushima, T., Minamiguchi, N., Hasui, Y., Osada, Y. and Kataoka, H. (2007) Clinical relevance of hepsin and hepatocyte growth factor activator inhibitor type 2 expression in renal cell carcinoma. *Cancer Sci.* **98**, 491–498
- Zacharski, L. R., Ornstein, D. L., Memoli, V. A., Rousseau, S. M. and Kiesel, W. (1998) Expression of the factor VII activating protease, hepsin, *in situ* in renal cell carcinoma. *Thromb. Haemostasis* **79**, 876–877
- Klezovitch, O., Chevillet, J., Mirosevich, J., Roberts, R. L., Matusik, R. J. and Vasioukhin, V. (2004) Hepsin promotes prostate cancer progression and metastasis. *Cancer Cell* **6**, 185–195
- Li, W., Wang, B. E., Moran, P., Lipari, T., Ganesan, R., Corpuz, R., Ludlam, M. J., Gogineni, A., Koeppen, H., Bunting, S. et al. (2009) Pegylated kunitz domain inhibitor suppresses hepsin-mediated invasive tumor growth and metastasis. *Cancer Res.* **69**, 8395–8402
- Hauske, P., Ottmann, C., Meltzer, M., Ehrmann, M. and Kaiser, M. (2008) Allosteric regulation of proteases. *ChemBioChem* **9**, 2920–2928

- 24 Hedstrom, L. (2002) Serine protease mechanism and specificity. *Chem. Rev.* **102**, 4501–4524
- 25 Cinader, B. and Lafferty, K. J. (1963) Antibody as inhibitor of ribonuclease: the role of steric hindrance, aggregate formation, and specificity. *Ann. N. Y. Acad. Sci.* **103**, 653–673
- 26 Xuan, J. A., Schneider, D., Toy, P., Lin, R., Newton, A., Zhu, Y., Finster, S., Vogel, D., Mintzer, B., Dinter, H. et al. (2006) Antibodies neutralizing hepsin protease activity do not impact cell growth but inhibit invasion of prostate and ovarian tumor cells in culture. *Cancer Res.* **66**, 3611–3619
- 27 Peterson, J. R. and Golemis, E. A. (2004) Autoinhibited proteins as promising drug targets. *J. Cell. Biochem.* **93**, 68–73
- 28 Oyen, D., Srinivasan, V., Steyaert, J. and Barlow, J. N. (2011) Constraining enzyme conformational change by an antibody leads to hyperbolic inhibition. *J. Mol. Biol.* **407**, 138–148
- 29 Ganesan, R., Eigenbrot, C., Wu, Y., Liang, W. C., Shia, S., Lipari, M. T. and Kirchhofer, D. (2009) Unraveling the allosteric mechanism of serine protease inhibition by an antibody. *Structure* **17**, 1614–1624
- 30 Stern, A. S. and Podlaski, F. J. (1993) Increasing the antigen binding capacity of immobilized antibodies. *Tech. Protein Chem.* **IV**, 353–360
- 31 Saldanha, S. W. (2007) *Handbook of Therapeutic Antibodies* (Dübel, S., ed.), pp. 119–144, Wiley-VCH, Weinheim
- 32 Lo, B. K. (2004) Antibody humanization by CDR grafting. *Methods Mol. Biol.* **248**, 135–159
- 33 Reference deleted
- 34 Lefranc, M. P., Giudicelli, V., Ginestoux, C., Jabado-Michaloud, J., Folch, G., Bellahcene, F., Wu, Y., Gemrot, E., Brochet, X., Lane, J. et al. (2009) IMGT, the international Immunogenetics information system. *Nucleic Acids Res.* **37**, D1006–D1012
- 35 Mundigl, O., Kaluza, K., Auer, H., Dürr, H., Georges, G., Jennewein, S., Ries, S. and Stracke, J. (2011) Anti-hepsin antibodies and methods of use. PCT/EP2011/060501, patent submitted
- 36 Kabsch, W. (2010) Xds. *Acta Crystallogr. Sect. D Biol. Crystallogr.* **66**, 125–132
- 37 McCoy, A. J., Grosse-Kunstleve, R. W., Adams, P. D., Winn, M. D., Storoni, L. C. and Read, R. J. (2007) Phaser crystallographic software. *J. Appl. Crystallogr.* **40**, 658–674
- 38 Soding, J., Biegert, A. and Lupas, A. N. (2005) The HHpred interactive server for protein homology detection and structure prediction. *Nucleic Acids Res.* **33**, W244–W248
- 39 Emsley, P., Lohkamp, B., Scott, W. G. and Cowtan, K. (2010) Features and development of Coot. *Acta Crystallogr. Sect. D Biol. Crystallogr.* **66**, 486–501
- 40 Blanc, E., Roversi, P., Vonrhein, C., Flensburg, C., Lea, S. M. and Bricogne, G. (2004) Refinement of severely incomplete structures with maximum likelihood in BUSTER-TNT. *Acta Crystallogr. Sect. D Biol. Crystallogr.* **60**, 2210–2221
- 41 Pettersen, E. F., Goddard, T. D., Huang, C. C., Couch, G. S., Greenblatt, D. M., Meng, E. C. and Ferrin, T. E. (2004) UCSF Chimera: a visualization system for exploratory research and analysis. *J. Comput. Chem.* **25**, 1605–1612
- 42 Brandstetter, H., Turk, D., Hoeffken, H. W., Grosse, D., Sturzebecher, J., Martin, P. D., Edwards, B. F. and Bode, W. (1992) Refined 2.3 Å X-ray crystal structure of bovine thrombin complexes formed with the benzamidine and arginine-based thrombin inhibitors NAPAP, 4-TAPAP and MQPA. A starting point for improving antithrombotics. *J. Mol. Biol.* **226**, 1085–1099
- 43 Wu, Y., Eigenbrot, C., Liang, W. C., Stawicki, S., Shia, S., Fan, B., Ganesan, R., Lipari, M. T. and Kirchhofer, D. (2007) Structural insight into distinct mechanisms of protease inhibition by antibodies. *Proc. Natl. Acad. Sci. U.S.A.* **104**, 19784–19789
- 44 Nemazee, D. A. and Sato, V. L. (1982) Enhancing antibody: a novel component of the immune response. *Proc. Natl. Acad. Sci. U.S.A.* **79**, 3828–3832
- 45 Ganesan, R., Eigenbrot, C. and Kirchhofer, D. (2010) Structural and mechanistic insight into how antibodies inhibit serine proteases. *Biochem. J.* **430**, 179–189
- 46 Sohn, J., Grant, R. A. and Sauer, R. T. (2007) Allosteric activation of DegS, a stress sensor PDZ protease. *Cell* **131**, 572–583
- 47 Wilken, C., Kitzing, K., Kurzbauer, R., Ehrmann, M. and Clausen, T. (2004) Crystal structure of the DegS stress sensor: how a PDZ domain recognizes misfolded protein and activates a protease. *Cell* **117**, 483–494
- 48 Horn, J. R. and Shoichet, B. K. (2004) Allosteric inhibition through core disruption. *J. Mol. Biol.* **336**, 1283–1291
- 49 Liu, S., Chang, J. S., Herberg, J. T., Horng, M. M., Tomich, P. K., Lin, A. H. and Marotti, K. R. (2006) Allosteric inhibition of *Staphylococcus aureus* D-alanine:D-alanine ligase revealed by crystallographic studies. *Proc. Natl. Acad. Sci. U.S.A.* **103**, 15178–15183
- 50 Maun, H. R., Eigenbrot, C. and Lazarus, R. A. (2003) Engineering exosite peptides for complete inhibition of factor VIIa using a protease switch with substrate phage. *J. Biol. Chem.* **278**, 21823–21830
- 51 Stanfield, R. L. and Wilson, I. A. (1994) Antigen-induced conformational changes in antibodies: a problem for structural prediction and design. *Trends Biotechnol.* **12**, 275–279
- 52 Freire, E. (1999) The propagation of binding interactions to remote sites in proteins: analysis of the binding of the monoclonal antibody D1.3 to lysozyme. *Proc. Natl. Acad. Sci. U.S.A.* **96**, 10118–10122
- 53 Gohara, D. W. and Di Cera, E. (2011) Allostery in trypsin-like proteases suggests new therapeutic strategies. *Trends Biotechnol.* **29**, 577–585
- 54 Huntington, J. A. (2008) How Na<sup>+</sup> activates thrombin: a review of the functional and structural data. *Biol. Chem.* **389**, 1025–1035
- 55 Kenakin, T. and Miller, L. J. (2010) Seven transmembrane receptors as shapeshifting proteins: the impact of allosteric modulation and functional selectivity on new drug discovery. *Pharmacol. Rev.* **62**, 265–304
- 56 Beckett, D. (2009) Regulating transcription regulators via allostery and flexibility. *Proc. Natl. Acad. Sci. U.S.A.* **106**, 22035–22036
- 57 Farady, C. J., Egea, P. F., Schneider, E. L., Darragh, M. R. and Craik, C. S. (2008) Structure of an Fab-protease complex reveals a highly specific non-canonical mechanism of inhibition. *J. Mol. Biol.* **380**, 351–360
- 58 Gille, C. and Frommel, C. (2001) STRAP: editor for STRuctural Alignments of Proteins. *Bioinformatics* **17**, 377–378
- 59 Edgar, R. C. (2004) MUSCLE: multiple sequence alignment with high accuracy and high throughput. *Nucleic Acids Res.* **32**, 1792–1797
- 60 Gouet, P., Courcelle, E., Stuart, D. I. and Metz, F. (1999) ESPript: analysis of multiple sequence alignments in PostScript. *Bioinformatics* **15**, 305–308
- 61 Huang, M., Furie, B. C. and Furie, B. (2004) Crystal structure of the calcium-stabilized human factor IX Gla domain bound to a conformation-specific anti-factor IX antibody. *J. Biol. Chem.* **279**, 14338–14346

## SUPPLEMENTARY ONLINE DATA

# Allosteric antibody inhibition of human hepsin protease

Tobias KOSCHUBS\*, Stefan DENGL†, Harald DÜRR†, Klaus KALUZA†, Guy GEORGES†, Christiane HARTL†, Stefan JENNEWEIN†, Martin LANZENDÖRFER†<sup>1</sup>, Johannes AUER†, Alvin STERN‡, Kuo-Sen HUANG‡, Kathryn PACKMAN‡, Ueli GUBLER‡, Dirk KOSTREWA\*, Stefan RIES†, Silke HANSEN†, Ulrich KOHNERT†, Patrick CRAMER\* and Olaf MUNDIGL†<sup>2</sup>

\*Gene Center Munich, Department of Biochemistry, Ludwig-Maximilians-Universität (LMU) München, Feodor-Lynen-Str. 25, 81377 Munich, Germany, †Roche Diagnostics GmbH, Roche Biologics Research, Nonnenwald 2, 82377 Penzberg, Germany, and ‡Roche, 340 Kingsland Street, Nutley, NJ 07110, U.S.A.

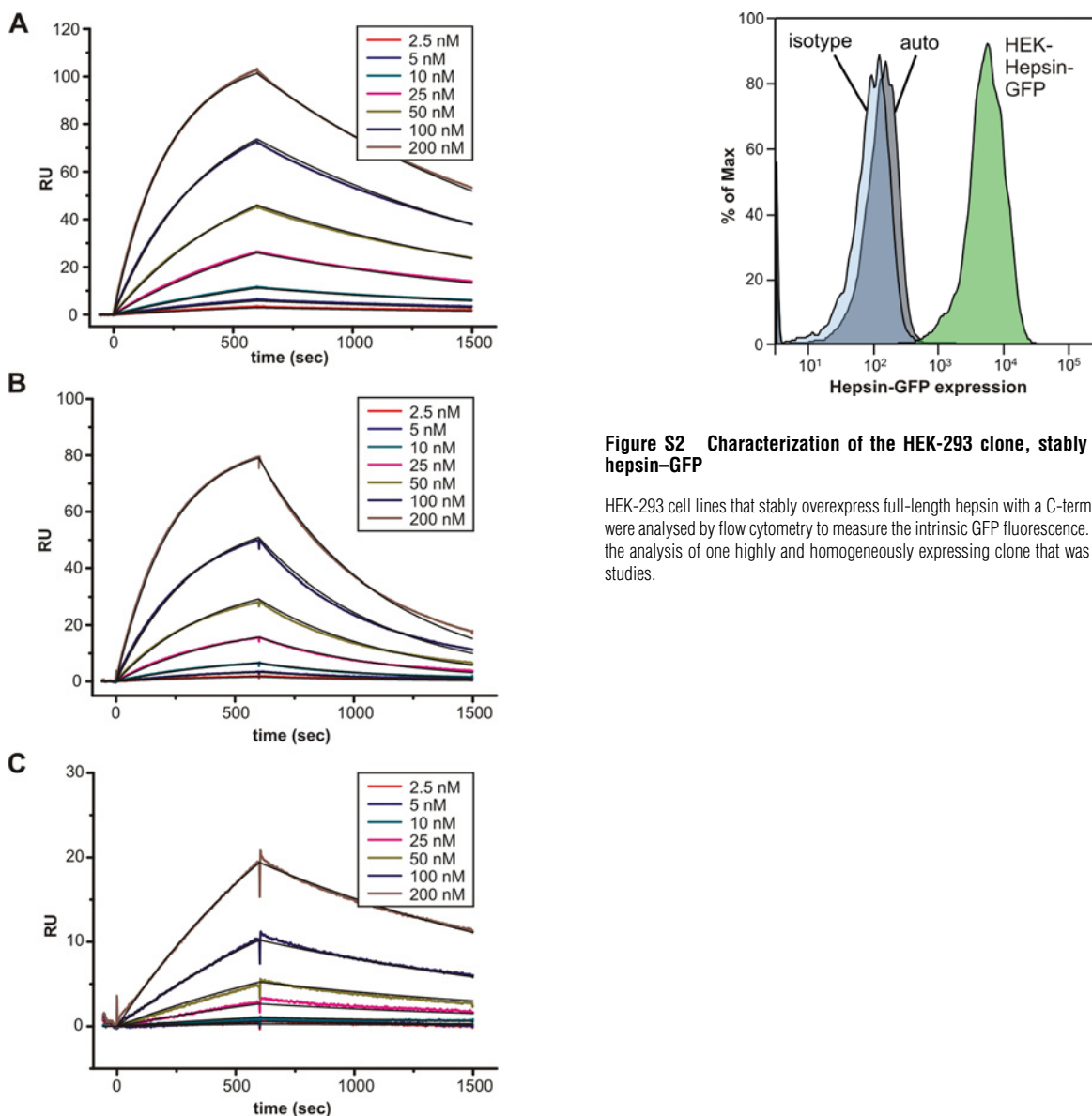


**Figure S2** Characterization of the HEK-293 clone, stably overexpressing hepsin-GFP

HEK-293 cell lines that stably overexpress full-length hepsin with a C-terminal GFP-fusion tag were analysed by flow cytometry to measure the intrinsic GFP fluorescence. The diagram shows the analysis of one highly and homogeneously expressing clone that was selected for further studies.

**Figure S1** Adjusted SPR (Biacore) sensograms

(A) Analysis of antibody hH35 immobilized via Protein A on a CM5 sensor chip. Hepsin was injected at concentrations 0–200 nM. Curve fittings using a 1:1 Langmuir binding model are shown by black lines. (B) Analysis of antibody chH35 immobilized via Protein A. Samples were measured and analysed analogously to (A). (C) Analysis of antibody mH35 immobilized via Protein G. Samples were measured and analysed analogously to (A).

<sup>1</sup> This paper is dedicated to the memory of the scientific integrity, passion and dedication of Martin Lanzendörfer, who died in September 2010, while at the peak of his career.

<sup>2</sup> To whom correspondence should be addressed (email olaf.mundigl@roche.com).

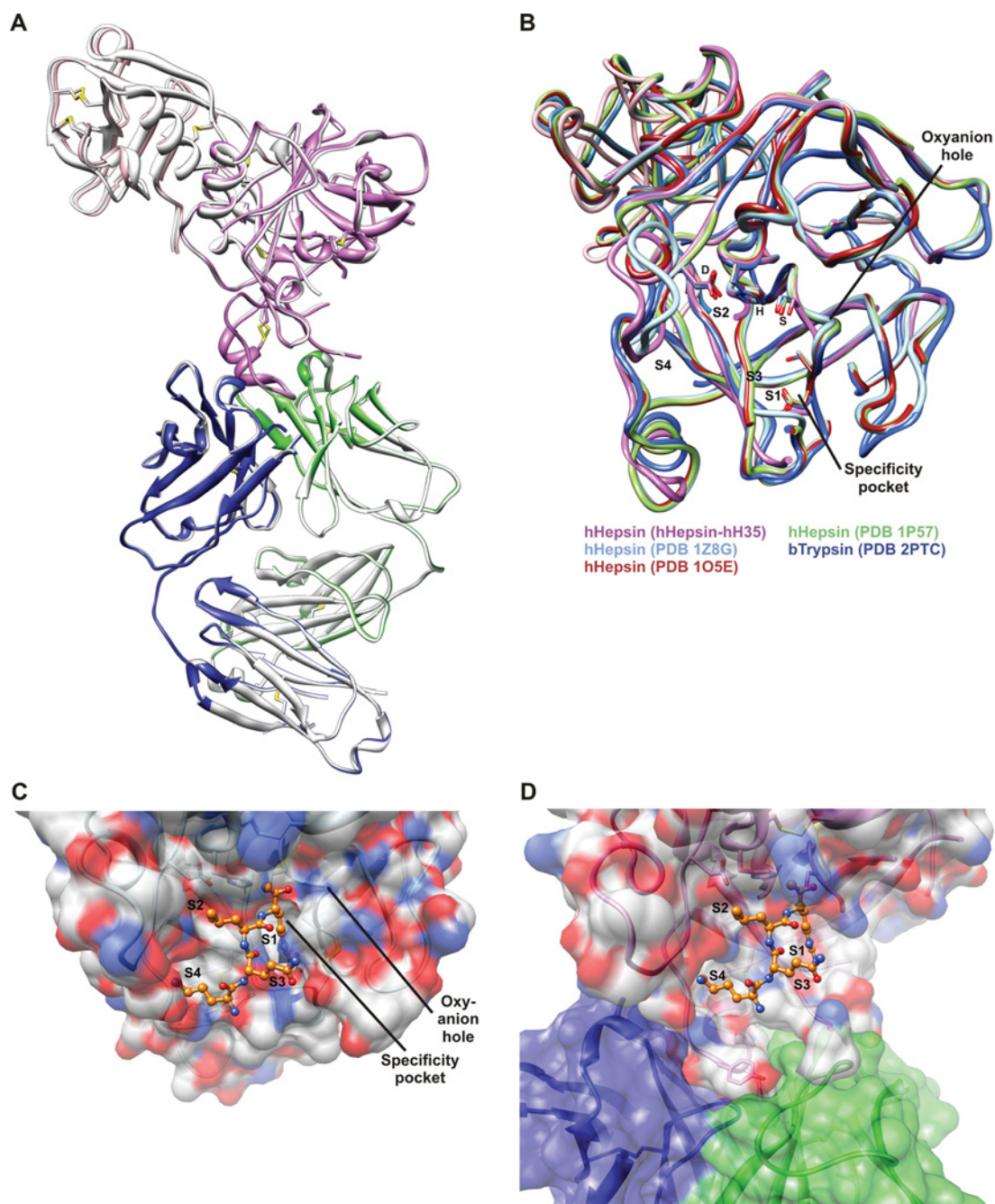


**Figure S3 Analysis of the protein hHepsin-hH35 Fab crystal structure**

(**A**) Ribbon-style model superimposition of the hHepsin-hH35 structure as shown in Figure 6(A) of the main text and the second NCS copy of hHepsin-hH35 present in the crystal unit cell (light grey). (**B**) Structural representation of hepsin in the hHepsin-hH35 complex superimposed on to other published hepsin structures and on bovine trypsin. Catalytic triad residues (aspartate, histidine and serine) are shown as sticks. Substrate-binding pockets are marked by S1-S4. (**C**) Semi-transparent surface view with an underlying ribbon model of human hepsin complexed with the KQLR-methylene ligand (shown in orange as a ball-and-stick representation) as found in the PDB code 1Z8G structure. Substrate-binding pockets are marked by S1-S4. (**D**) Semi-transparent surface view with an underlying ribbon model of the hHepsin-hH35 complex structure. A hypothetical model complex with the KQLR-methylene ligand (based on the superimposition on to the PDB code 1Z8G structure) is shown.

CDR	H-Bonds NCS copy 1			H-Bonds NCS copy 2		
	Fab hH35	Hepsin	Distance (Å)	Fab hH35	Hepsin	Distance (Å)
CDR-L1	THR 29 [OG1]	GLN 385 [NE2]	3.9	THR 29 [OG1]	GLN 385 [NE2]	3.6
				TYR 32 [OH]	TYR 341 [N]	3.9
CDR-L2	ASP 50 [O]	GLN 385 [N]	3.4	ASP 50 [O]	GLN 385 [N]	3.2
	ASN 52 [OD1]	GLN 385 [N]	3.3	ASN 52 [OD1]	GLN 385 [N]	3.4
	ASN 53 [ND2]	LEU 383 [O]	2.8	ASN 53 [ND2]	TYR 328 [OH]	3.9
CDR-H1	ARG 54 [O]	TYR 328 [OH]	3.3	ARG 54 [O]	TYR 328 [OH]	3.2
	ASP 31 [O]	GLN 331 [N]	3.7	ASP 31 [O]	GLN 331 [N]	3.5
	ASP 31 [O]	LYS 333 [NZ]	3.6			
	SER 33 [N]	GLY 329 [O]	2.6	SER 33 [N]	GLY 329 [O]	2.8
CDR-H2	ARG 35 [NH2]	ASP 326 [O]	2.4	ARG 35 [NH2]	ASP 326 [O]	2.4
	THR 52A [N]	GLN 331 [OE1]	2.9	THR 52A [N]	GLN 331 [OE1]	2.9
CDR-H3	PHE 96 [N]	PHE 327 [O]	2.6	PHE 96 [N]	PHE 327 [O]	2.7
	ALA 101 [N]	PHE 327 [O]	3.0	ALA 101 [N]	PHE 327 [O]	3.1
Other-H	THR 30 [O]	GLN 331 [NE2]	3.0	THR 30 [O]	GLN 331 [NE2]	2.8
	ARG 94 [NH2]	TYR 328 [O]	3.6	ARG 94 [NH1]	TYR 328 [O]	3.6

CDR	Salt bridges NCS copy 2		
	Fab hH35	Hepsin	Distance (Å)
CDR-H1	ASP 31 [OD1]	LYS 333 [NZ]	3.8

CDR	Hydrophobic interactions NCS copy 1		Hydrophobic interactions NCS copy 2	
	Fab hH35	Hepsin	Fab hH35	Hepsin
CDR-L1	TYR 32	ILE 317	TYR 32	ILE 317
		GLY 324		
		ALA 325		
		GLY 340		
		TYR 341		
		PRO 387		
CDR-L2	ALA 55	PHE 327	ALA 55	PHE 327
		TYR 328		TYR 328
CDR-L3	TRP 91	VAL 321	TRP 91	VAL 321
		GLY 324		GLY 324
Other-L	PHE 96	ALA 325	PHE 96	ALA 325
		GLY 324		GLY 324
		ALA 325		ALA 325
		TRP 35		PHE 327
		GLY 46		PHE 327
		LEU 47		PHE 327
CDR-H1	TYR 32	PHE 327	TYR 32	
		TYR 328		TYR 328
		GLY 329		GLY 329
		ILE 317		
		GLY 324		GLY 324
CDR-H2	TRP 50	ALA 325	TRP 50	
		PHE 327		PHE 327
		TYR 328		TYR 328
		GLY 329		GLY 329
		ALA 325		
		PHE 327		PHE 327
CDR-H3	GLY 95	TYR 328	GLY 95	TYR 328
		GLY 329		GLY 329
		ALA 325		
		PHE 327		PHE 327
		TYR 328		TYR 328
		GLY 329		GLY 329
Other-H	TRP 47	ALA 325	TRP 47	
		PHE 327		PHE 327
		TYR 328		TYR 328
		TYR 102		TYR 328
		GLY 324		GLY 324

Figure S4 Continued

CDR	Crystal contacts NCS copy 1			Crystal contacts NCS copy 2		
	Fab hH35	Hepsin	Distance (Å)	Fab hH35	Hepsin	Distance (Å)
Other-L	GLN 1 [N]	SER 213 [O]	3.2	GLN 1 [NE2]	ARG 214 [O]	3.0
	THR 18 [OG1]	ARG 124 [NH1]	3.6			
	VAL 159 [O]	ARG 208 [NH1]	3.6	VAL 159 [O]	ARG 208 [NH1]	3.0
				GLY 199 [O]	THR 128 [N]	3.8
				THR 201 [OG1]	ARG 124 [NE]	3.6
CDR-H1				TYR 32 [OH]	GLU 252 [OE2]	3.2
CDR-H2				ASP 61 [O]	SER 411 [OG]	3.6
	ASP 62 [OD1]	SER 213 [N]	3.5	ASP 62 [OD1]	LEU 212 [N]	3.8
	ASP 62 [OD1]	SER 213 [OG]	2.8	ASP 62 [OD1]	SER 213 [N]	3.3
	ASP 62 [OD2]	SER 213 [OG]	3.0	ASP 62 [OD2]	SER 213 [OG]	2.6
Other-H	GLN 43 [OE1]	ARG 214 [NH2]	3.9			
	LYS 83 [NZ]	MET 413 [O]	3.7	LYS 83 [NZ]	MET 413 [O]	3.5
	GLU 85 [OE1]	ARG 210 [NH2]	2.8	GLU 85 [OE1]	ARG 210 [NH2]	2.9
Other-L	GLU 160 [OE2]	ARG 208 [NH1]	3.7	GLU 160 [OE1]	ARG 208 [NH1]	3.4
Other-H	GLU 85 [OE1]	ARG 210 [NE]	3.9	GLU 85 [OE1]	ARG 210 [NE]	4.0
	GLU 85 [OE1]	ARG 210 [NH2]	2.8	GLU 85 [OE1]	ARG 210 [NH2]	2.9

**Figure S4 Residue contact analysis between hH35 Fab fragment and human hepsin**

Residue contacts between the hH35 Fab fragment and human hepsin were analysed using CCP4 CONTACT [4] and PISA [5] software.

**Table S1  $K_m$  values of serine proteases using the acetyl-KQLR-AMC peptide as a substrate**

Values are means  $\pm$  S.D., from at least three independent tests performed in triplicate. The  $K_m$  in column two refers to KQLR as the substrate, whereas the  $K_m$  in column four refers to the referenced 'ideal' substrate.

Enzyme	Apparent $K_m$ ( $\mu M$ ) <sup>*</sup>	Ideal peptide substrate <sup>†</sup>	Apparent $K_m$ ( $\mu M$ )	Reference
Hepsin	10.1 $\pm$ 0.8			
Trypsin	34.0 $\pm$ 2.4	N <sup>alpha</sup> -p-Tos-Gly-Pro-Lys-AMC	14	[1]
Trypsin	34.0 $\pm$ 2.4	Boc-Phe-Ser-Arg-4-MCA	16.5 $\pm$ 0.9	[2]
Bovine enteropeptidase	22.2 $\pm$ 1.2	Trypsinogen	5.6 $\pm$ 0.9	[3]
HAT	123.6 $\pm$ 16.3	ABZ-Arg-Gln-Asp-Arg-ANB-NH <sub>2</sub>	25.4 $\pm$ 2.1	[2]
Matriptase	26.5 $\pm$ 2.7	ABZ-Arg-Gln-Asp-Arg-ANB-NH <sub>2</sub>	68.5 $\pm$ 4.2	[2]
Matriptase	26.5 $\pm$ 2.7	Boc-Phe-Ser-Arg-4-MCA	12.1 $\pm$ 1.9	[2]

<sup>\*</sup>Hydrolysis rates of at least six different peptide concentrations were monitored for determination of the apparent  $K_m$  values. Data were fitted to the Michaelis–Menten equation.

<sup>†</sup>As reported in the stated references.

**Table S2 Initial ( $v_0$ ) and steady-state ( $v_s$ ) velocities of Figure 4(C) (in the main text) measurements**

Measurement	$v_0$ (nM $\cdot$ s <sup>-1</sup> )	$v_s$ (nM $\cdot$ s <sup>-1</sup> )
No hH35	12.8	11.8
18 nM hH35	12.1	10.4
55 nM hH35	11.8	7.8
166 nM hH35	9.2	4.0
500 nM hH35	6.8	1.2

**Table S3 Comparison of different inhibition models**

The calculated results are ranked according to the  $R^2$  equation. AICc, Akaike information criterion with a correction for finite sample size; Sy,x, S.D. of the residuals.

Rank by runs	Equation*	$R^2$	AICc	Sy,x	Test	Convergence
1	Mixed Tight	0.99553	− 933.779	1.13E − 02	Pass	Yes
2	Non-competitive Tight	0.99549	− 935.124	1.13E − 02	Pass	Yes
3	Competitive Tight	0.99273	− 885.02	1.43E − 02	Pass	Yes
4	Uncompetitive Tight	0.99063	− 858.376	1.63E − 02	Pass	Yes

\*Study type: tight-binding inhibition with three replicates, fitted in SigmaPlot®.

## REFERENCES

- 1 Evin, L. B., Vasquez, J. R. and Craik, C. S. (1990) Substrate specificity of trypsin investigated by using a genetic selection. *Proc. Natl. Acad. Sci. U.S.A.* **87**, 6659–6663
- 2 Wysocka, M., Spichalska, B., Lesner, A., Jaros, M., Brzozowski, K., Legowska, A. and Rolka, K. (2010) Substrate specificity and inhibitory study of human airway trypsin-like protease. *Bioorg. Med. Chem.* **18**, 5504–5509
- 3 Zheng, X. L., Kitamoto, Y. and Sadler, J. E. (2009) Enteropeptidase, a type II transmembrane serine protease. *Front. Biosci.* **1**, 242–249
- 4 Collaborative Computational Project, number 4 (1994) The CCP4 suite: programs for protein crystallography. *Acta. Crystallogr. Sect D Biol. Crystallogr.* **50**, 760–763
- 5 Krissinel, E. and Henrick, K. (2007) Inference of macromolecular assemblies from crystalline state. *J. Mol. Biol.* **372**, 774–797

Received 22 July 2011/22 November 2011; accepted 2 December 2011

Published as BJ Immediate Publication 2 December 2011, doi:10.1042/BJ20111317